**Light Metals 2015**
*Edited by: Margaret Hyland*
***TMS (The Minerals, Metals & Materials Society), 2015***

# Study on the Dissolution of Alumina in Cryolite Electrolyte Using the See-Through Cell

Youjian Yang, Bingliang Gao, Zhaowen Wang, Zhongning Shi, Xianwei Hu
School of Materials and Matallurgy, Northeastern University, Mail Box 117, Shenyang, China

Keywords: Alumina, Dissolution, Cryolite electrolyte, See through cell

## Abstract

By using the see-through cell, the dissolution phenomenon of alumina in the cryolite electrolyte was clearly visible. In this paper, the dissolution processes of primary and secondary alumina in typical aluminum bath were shown and the dissolution rates were compared as well as the temperature fluctuations during dissolution. Both the video and temperature measurements confirm the three key steps of the dissolution process: fast dissolution upon feeding, crust formation and sludge dissolution. And the dissolution rate in each step is very different. Secondary alumina displays a quite different dissolution behavior from primary alumina. Meanwhile, the dissolution rate of secondary alumina is much faster than that of primary alumina. The mechanism for alumina dissolution under the influences of MOI, LOI, surface area, absorbed fluorine and carbon content was also discussed.

## Introduction

Smelting grade alumina is used as the raw material for industrial aluminum electrolysis. Modern smelter potlines often undergo a series of negative effects which could be partly attributed to the dissolution problems of alumina. The poor dissolution of alumina could cause instability of the cell condition by increasing the bath resistivity (pseudo resistance of dissolved alumina), the amount of cell sludge and the probability of local anode effect. As a result, the cell would be running under lower efficiency and changed heat balance.[1] In order to keep the electrolysis stable, it is necessary to maintain the optimum concentration and distribution of the alumina in the cell. In other words, the dissolving conditions of alumina may impact this dynamic balance. The use of the primary alumina as an absorbent for recycling the gaseous and particulate emissions in dry scrubbers also put forward requests to the adsorption capacity of alumina.[2]

This paper, introduces the method of see-through cell for observing, measuring, comparing the dissolution behavior of industrial grade alumina. The influences of alumina properties on cell operation are analyzed and summarized based on the results of this work combined with other researchers' results.

## Experimental

Chemicals

Analytical reagents, calcium fluoride, lithium fluoride and chemical pure reagent cryolite were dried at 400°C for 2h. Chemical pure reagent aluminum fluoride trihydrate was mixed with ammonium hydrogen fluoride at a fixed mass ratio of 7:3 and dried for 2h at 150 °C and 250°C, respectively, and then kept for at least 3h at 500°C to remove structural water.[3] All the chemicals were kept in a dry box before use.

Primary alumina and secondary alumina (containing 0.55wt% fluorine and 0.52wt% carbon) used in the experiments were taken from an alumina refinery, had average grain sizes of 70.12um and 68.46um, respectively, and thus both belonged to intermediate alumina. The LOI (300-1000) of the primary and secondary alumina were 0.8wt% and 1.0wt%, respectively. All the experiments adopted a same bath composition: 83% $Na_3AlF_6$ - 8% $AlF_3$ - 5% LiF - 4% $CaF_2$, with a liquidus temperature of 951°C.

Experimental method and apparatus

The experimental apparatus for observing dissolution behavior was a see-through cell, as shown in Figure 1. The cell was made of high-purity quartz, and had dimensions of 55mm × 55mm × 80mm, with a wall thickness of 3mm. The cell was located in a heat-resistant furnace, two sides of which were fitted with identical quartz glass windows. A sunlamp was placed at the rear window to provide backlighting, and a video camera (MV-VS078FC) near the front window recorded the process inside the crucible. A temperature controller (DWT-702) with a Pt-PtRh10 type thermocouple was used to measure and control the furnace temperature.

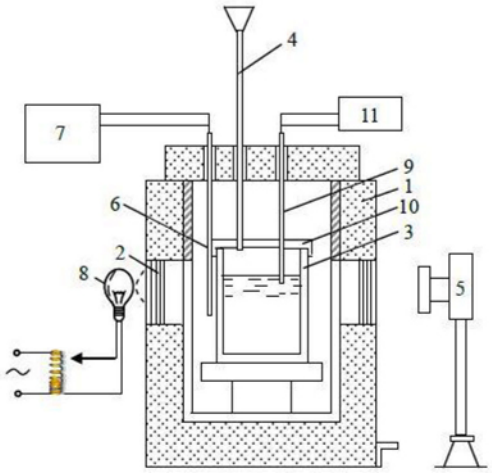


1. electric-resistance furnace, 2. quartz glass window, 3. quartz crucible, 4. charging pipe, 5. camera, 6. thermocouple, 7. temperature controller, 8. adjustable light source, 9. thermocouple, 10. stainless steel cap, 11. temperature measurement module

Fig.1 The experimental apparatus of the transparent cell

The electrolyte weight in each run was 200 grams. The molten electrolyte height was 5.5cm, and the electrolyte temperature was controlled at 955 (±1)°C during the experiments, which represented initial superheat of about 4°C. 2 grams of alumina was charged into the transparent molten salt for each run through a corundum tube with its end positioned 2cm above the electrolyte surface. Before and after every addition, the tube was dredged with a stainless steel stick to clear any blockage.

Another Pt-PtRh10 type thermocouple was immersed in the molten bath at a depth of 1cm below the melt surface to measure

the temperature fluctuation of the electrolyte during feeding. A NI-USB-9162 type temperature measurement module from National Instruments was used to collect the signal at a frequency of 4Hz. The quartz crucible can hold on the electrolyte for about 2 hours at 955°C without leakage and losing its transparency. The maximum $SiO_2$ content in the melts after the experiment was 0.12wt%, which was insufficient to significantly affect the results of alumina dissolution and electrolyte composition.

## Results and Discussion

The Dissolution Behavior of Primary Alumina

By using the see-through cell, the dissolution phenomenon of alumina samples was recorded. Key pictures during primary alumina dissolution are shown in Figure 2.

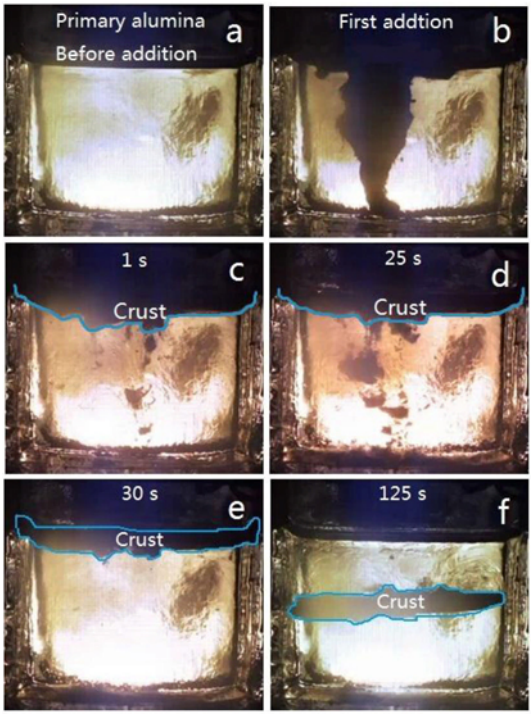


Figure 2 Key pictures during the dissolution of primary alumina (2g alumina powder in 200g electrolyte, 955°C, superheat=4°C)

At the moment of feeding, a portion of alumina powder was able to reach the bottom of the crucible due to the inertia force as it was dropped from the feeding pipe (Fig. 2a). But immediately (within 1 seconds, Fig. 2b), the alumina powder returned to the surface because of its lower apparent density contrast to the molten cryolite. At the same time, part of the alumina particles began to disperse and dissolve rapidly into the electrolyte. Meanwhile, the crust, which was the mixture of condensed electrolyte and alumina particles were formed. This process lasted for approximately 30 seconds, meanwhile the temperature of the electrolyte dropped to a lowest value (Fig. 2c, 2d, 2e, Fig. 3). In the following 95 seconds, the 'boat-like' crust floated steadily and dissolved slowly at the surface. 125 seconds after addition, the crust was totally soaked with bath and sank to the crucible bottom (Fig. 2f). The crust dissolved very slowly and the crucible did not become clear again until 480 seconds later. The shape of the crust did not change a lot since 1 second after addition, which suggests that the crust was formed at the very beginning of feeding.

Temperature Fluctuation during Alumina Dissolution

The temperature fluctuation of the electrolyte during alumina dissolution was measured and shown in Figure 3. Firstly, when 2 grams of alumina sample were added to the electrolyte, heat transfer from molten melts to cold alumina particles was used to preheat the sample and supply heat for the endothermic dissolution reaction, the fed alumina also underwent an exothermic phase transitions from gamma phase to alpha phase. This resulted in a sudden 5°C decrease of the bath temperature in the first 30 seconds. The temperature gradually increased with the soaking of the agglomerate. Finally, 120 seconds after feeding, the soaked agglomerate sank to the bottom of the crucible, corresponding to the cooling peak at 120s in Figure 3.[4] The second feeding was made at 1000 seconds and the temperature curve showed the same style.

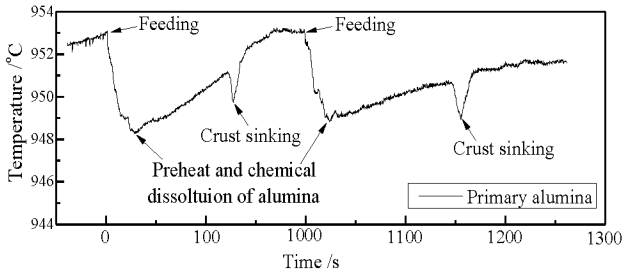


Figure 3 Temperature fluctuation caused by 1pct (2g) addition of primary alumina, 955°C, superheat=4°C[4]

The Dissolution Rate of Primary Alumina

The dissolution time of each feeding was calculated from the moment the alumina reached the surface of the electrolyte until the bottom of the crucible became clearly visible. The next feeding was made when the temperature fluctuation of the melt remained below 1°C for 10 minutes. Figure 4 shows the accumulated dissolution time of multiple additions of faster and slower dissolving alumina, respectively. Alumina sample with faster dissolution rate is also marked in Figure 4. The sum of dissolution time of the first three/four additions could be used to distinguish the dissolution capacity of different alumina samples. Generally, the smelters do not want alumina sink quickly as added because this would increase the risk of bottom sludge.[5] The average floating time of different alumina samples is also comparable using this system.

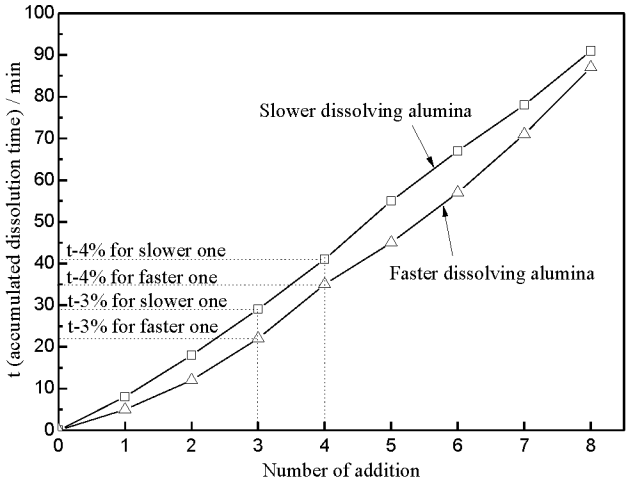


Figure 4 The accumulated dissolution time of two different

alumina samples. t-3% stands for the overall dissolution time of the first three additions, similarly, t-4% stands for the overall dissolution time of the first four additions, 955°C, superheat=4°C

According to the authors' earlier studies and results of other researchers, the significances of some alumina specifications are listed in Table1.

Table 1 Primary alumina specifications and their influences on cell operation

| Parameters | Physical Significance | Influence on Cell Operation |
|---|---|---|
| Purity | Do not introduce excess contaminant; maintain the purity of the bath composition and product aluminum. | Fe, Si, V would reduce the current efficiency and purity of the product aluminum; Na, Ca, Li, K, would change the bath composition. |
| LOI(25-300) | Absorbed moisture content, or called moisture on ignition (MOI), contributes to HF emission by hydrolyzing with pot fume.[6] | Change with ambient humidity[7], helpful to the dispersion of alumina particles upon feeding, beneficial to alumina dissolution rate[8]. |
| LOI(300-1000) | Structural hydroxyl content, major source of HF emission[6], describes the overall degree of phase transitions, closely related to Surface Area and Alpha Content.[9] | Hydroxyl introduced in this way could have a long lasting time in the bath[10], providing a continuous HF background; beneficial to the dissolution rate. |
| Bulk Density | Approximately 1g/cm$^3$, affect the accuracy of actual volumetric feeding. | Supposed to reduce the floating time of fed alumina a little bit if increased due to the difference in density with liquid bath. |
| B.E.T. Surface Area | Potential capacity for the absorption of gaseous HF, bath volatiles, carbon dust and other particulates[2]. | Larger surface area is beneficial to the dissolution rate by increasing the contact area between alumina particles and liquid bath[8]. |
| Attrition Index | Degree of the fraction resistance during the pipeline transportation and dry scrubbing system. | Contribute to the dust loss during feeding, harmful to the environment of the pot room. |
| Alpha Content | The amount of the most stable and indissolvable alumina phase. Closely related to LOI (300-1000) at the same calcination strategy. | Usually controlled below 10%, this part of alumina dissolves slowly, would possibly translate into bottom sludge. |
| Dust Index | Fine particles content, the percentage of particles with grain size below 30um. Assessment of the dust loss during transportation and feeding. | Describe the ability to be transported away from the cell in the form of suspending dust in the air[11]. |
| Average Grain Size | Comprehensive assessment of the manufacturing technique. Closely related to LOI(300-1000), BET surface area and Alpha content. Greatly influenced by the leaching technology and calcine process of gibbsite. | Larger grain size is expected, which usually indicates accompanying larger surface area, lower alpha content, less fine particles, smaller angle of repose, shorter flow funnel time and faster dissolution rate[12]. |
| Angle of Repose | Measure of the flowablity of the alumina particles, describes the ability to be transported through pipeline, fill the storage vessels and disperse upon feeding. Influenced by LOI(25-300).[1] | Smaller angle of repose indicates less blockage of the feeding system, no volcanic effect at the feeding point and faster dissolution rate. |
| Flow Funnel Time | Another measure of the flowability of the alumina. | Same as 'Angle of Repose'. |

The Dissolution Behavior of Secondary Alumina

Secondary alumina is the byproduct of the dry scrubbing process for recycling valuable fluorides from cell fume after using primary alumina as the absorbent. Contrast to primary alumina, secondary alumina contains more impurities including chemisorbed HF, physisorbed volatiles ($AlF_3$, $Na_5Al_3F_{14}$ and $Na_3AlF_6$, mainly from the decomposition of $NaAlF_4$ at low temperature), entrained bath (same composition as the electrolyte), carbon dust (generated from the selective burning of carbon anodes), and little sulfur, phosphor from anode impurities.[13]

The key pictures during secondary alumina dissolution are shown in Figure 5. Same as the dissolution of primary alumina, alumina powder began to disperse and dissolve rapidly immediately after feeding (Fig. 5b), this process did not seem to be weakened (Fig.5c) after 30 seconds. From the snapshot of 80 seconds and 130 seconds, it was clearly visible that small pieces of crust were sinking and dispersing in the electrolyte (marked in Fig. 5d,5e). 180 seconds later, the crucible became clear again. No big piece of crust was observed in the whole dissolution process or in the subsequent repetitive additions.

Figure 6 shows the accumulated dissolution time of secondary alumina and primary alumina in their respective experiments. The secondary alumina used in the experiments contained 0.55wt% fluorine and 0.52wt% carbon. It can be seen that the secondary alumina spent less time on dissolving the same amount of alumina (2 grams each time) contrast to primary alumina. Considering the t-3% and t-4% marked in Figure 6, in this case, the dissolution rate of secondary alumina is nearly 50% faster than that of primary alumina.

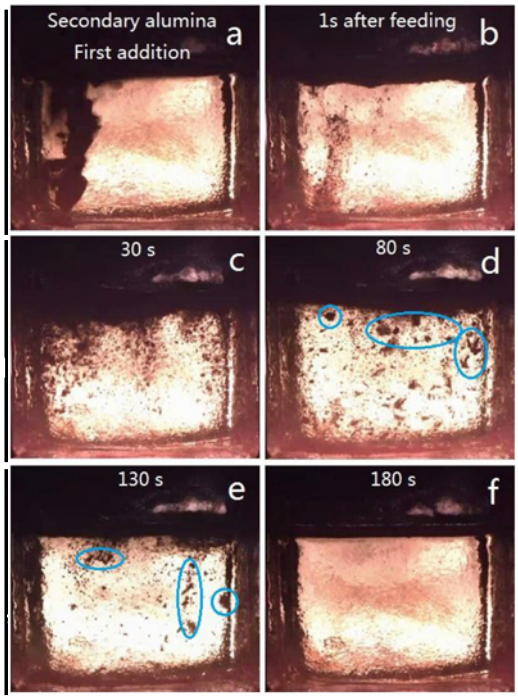


Figure 5 Key pictures during the dissolution of secondary alumina (955°C, superheat=4°C, 2g alumina powder in 200g electrolyte, small pieces of crust were formed as marked in Fig.5d and 5e, contrast to one giant crust during the dissolution of primary alumina in Figure 2f.)

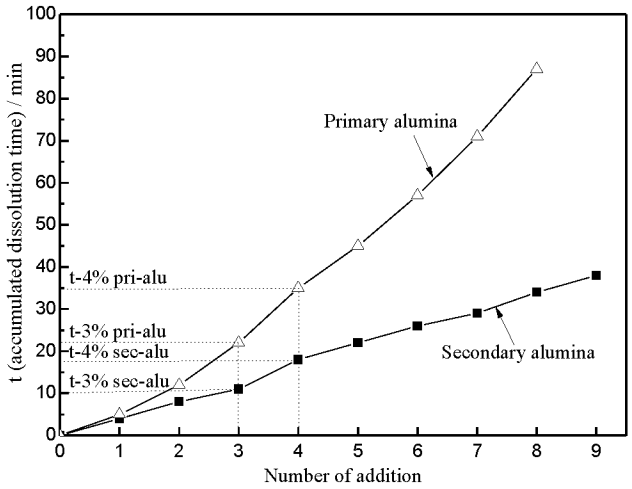


Figure 6 The accumulated dissolution time of primary alumina vs. secondary alumina, 955°C, superheat=4°C, 200g electrolyte, 2g alumina each time

Measurement of the temperature fluctuations during primary and secondary alumina dissolution also showed the same principle. Figure 7 shows the temperature fluctuations during primary and secondary alumina dissolution respectively. A thermo compressed BN protection tube was put on the head of the S type thermocouple to prevent the interference of the carbon content (one of the impurities in secondary alumina) to the exposed platinum thermocouple head. Subsequently, this corresponded to the loss of accuracy and introduced interruption (less than 0.6°C) from bubbles generated by the BN tube. It can be seen that carbon absorbed in secondary alumina burned instantly after feeding, which preheated the alumina particles to a certain extent. This made the initial temperature drop for secondary alumina feeding (2.5°C) 0.5°C less than that of primary alumina (3°C)[4]. During the dissolution of secondary alumina, the temperature of the electrolyte recovered faster than that of primary alumina, which suggests the dissolution of secondary alumina finished earlier.

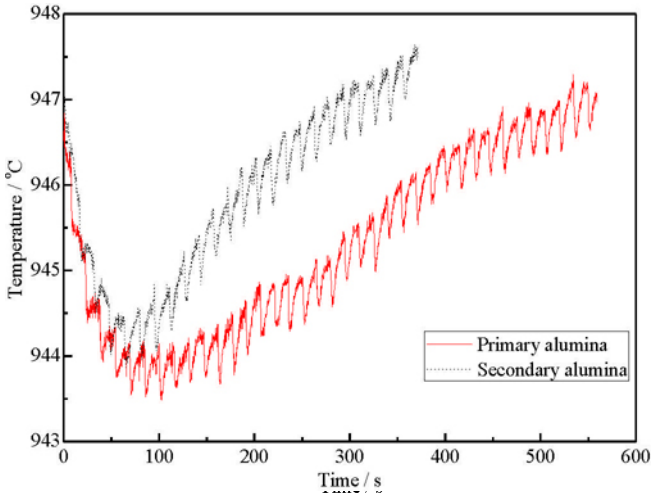


Figure 7 Temperature fluctuations during primary and secondary alumina dissolution respectively, 955°C, superheat=4°C, 2g alumina powder in 200g electrolyte[4]

The influences from dry scrubbing process on secondary alumina dissolution are summarized and listed in Table 2.

Table 2 Changes on alumina properties after dry scrubbing process and their influences on cell operation

| Change | Cause of formation | Influence on Cell Operation |
|---|---|---|
| Increase of the LOI(25-300) | Physisorption of moisture from large amount of air and flash off water from earlier fed alumina. | Contributes to HF emission by hydrolyzing with cell fume, helpful to the dispersion of alumina particles upon feeding, beneficial to alumina dissolution rate. |
| Appearance of chemisorbed HF, part of the –OH (hydroxyl) in alumina was replace by –F to form –OF or –F. Increase of the $AlF_3$ content. | Chemisorption of the gaseous HF emission from the cell exhaust. | Supposed to accelerate the alumina dissolution rate by shortening the steps of forming $[Al_xOF_y]^{(2-3x+y)-}$, which essentially is the dissolution reaction of alumina in aluminum electrolyte[14], but not observed in experiments. |
| Appearance of fluoride impurities including $AlF_3$, $Na_5Al_3F_{14}$ and $Na_3AlF_6$ (total fluorine content including chemisorbed HF generally varies from 0.2 pct to 1.2 pct) | Physisorption of bath volatiles (mainly $AlF_3$ and $NaAlF_3$ which decomposed into $AlF_3$, $Na_5Al_3F_{14}$ and $Na_3AlF_6$ at low temperature) and entrained bath (mainly $Na_5Al_3F_{14}$ and $Na_3AlF_6$). | Very small amount of fluoride has little effect on the dissolution rate of alumina.[4] |
| Appearance of carbon dust (generally from 0.3 pct to 1.0 pct) | Physisorption of carbon dust entrained in the cell fume, carbon dust was formed due to the select oxidation of carbon anode when it was exposed to the air. | Burning of carbon dust upon feeding could preheat and introduce gas agitation to alumina particles, which accelerate alumina dissolution rate by inhibiting the formation of giant crust.[4, 13] |
| Appearance of impurities like Si, Fe, S and P etc. | Physisorption of other particulates, COS and $SO_2$, etc. Generally introduced by petroleum cokes used in anode manufacturing. | Fe, Si, V, P would reduce the current efficiency and purity of the product aluminum; Most of the COS and $SO_2$ would go through the dry scrubber and escape into the atmosphere.[15] |

## Conclusion

The method of see-through cell for observing the dissolution behavior of alumina in cryolite electrolyte is introduced and the results of earlier studies are summarized in this paper. The influence of alumina specifications on the dissolution rate of primary alumina and the effects of dry scrubbing system on the dissolution rate of secondary alumina are listed as well. To avoid the problem of alumina dissolution, the smelters are expected to select alumina with better specification parameters. With the development of Bayer process technology and large scale aluminum cell technology, a new series of critical standards for alumina specifications have to be reached an agreement on between modern smelters and alumina refining plants.

## Acknowledgements

The authors would like to express their gratitude for the financial support provided by the National Key Technology Research and Development Program of the Ministry of Science and Technology of China (Grant No. 2012BAE08B01), the National Natural Science Foundation of China (Grant No. 51074045, 51228401, 51322406, 51434005, 51474060).

## References

1. B. Welch and G. Kuschel, "Crust and alumina powder dissolution in aluminum smelting electrolytes," *JOM*, 59(5), 2007: p. 50-54.
2. B. Welch and N. Wai-Poi, "Comparing alumina quality specifications and smelter expectations in cells," *Light Metals*, TMS, 1994: 345-350.
3. J. Tie, Z. Qiu and G. Lu, "A new method of preparing anhydrous aluminum fluoride," *Non-ferrous Metal*, 46(2), 1994: 49-51.
4. Y. Yang, B. Gao, Z. Wang, Z. Shi, X. Hu and J. Yu, "Dispersion caused by carbon dioxide during secondary alumina dissolution: a lab-scale research," *Metallurgical and Materials Transactions B*, 45(3), 2014.: 1150-1156.
5. A. R. Johnson, "Alumina crusting and dissolution in molten electrolyte," *Light Metals*, TMS, 1981: 373-387.
6. Y. Yang, M. Hyland, C. Seal and Z. Wang, "Modelling HF generation: the role of ambient humidity," *Light Metals*, TMS, 2014: 641-646.
7. M. Hyland, A. Gillespie and J. Metson, "Predicting moisture content on smelter grade alumina from measurement of the water isotherm," *Light Metals*, TMS, 1997: 113-117.
8. G. Kuschel, "The effect of alumina properties and smelter operating conditions on the dissolution behaviour of alumina," *PhD thesis, in Chemical and Materials Engineering, University of Auckland, Auckland, New Zealand*, 1990.
9. G. Paglia, "Determination of the structure of y-alumina using empirical and first principle calculations combined with supporting experiments," *PhD thesis, in Department of Applied Physics and Department of Applied Chemistry. Curtin University of Technology, Perth, Australia*, 2004.
10. M. Hyland, M. E. Patterson and B. Welch, "Alumina structural hydroxyl as a continuous source of HF," *Light Metals*, TMS, 2004: 361-366.
11. D. S. Wong, N. I. Tjahyono and M. M. Hyland, "Visualising the sources of potroom dust in aluminium smelters," *Light Metals*, TMS, 2012: 833-838.
12. L. M. Perander, "Evolution of nano-and microstructure during the calcination of Bayer gibbsite to produce alumina," *PhD thesis, in Chemical and Materials Engineering, University of Auckland, Auckland, New Zealand*, 2010.

13. Y. Yang, B. Gao, Z. Wang, Z. Shi and X. Hu, "Mechanism of dissolution behavior of the secondary Alumina," *Metallurgical and Materials Transactions B*, 44(5), 2013: 1296-1303.
14. X. Hu, J. Qu, B. Gao, Z. Shi, F. Liu and Z. Wang, "Raman spectroscopy and ionic structure of $Na_3AlF_6$-$Al_2O_3$ melts," *Transactions of Nonferrous Metals Society of China*, 21(2), 2011: 402-406.
15. M. Hyland, B. Welch and J. Metson, "Changing knowledge and practices towards minimising fluoride and sulphur emissions from aluminium reduction cells," *Light Metals*, TMS, 2000: 333-338.